# xCT as a potential marker for neuroendocrine cells in high-risk prostate cancer and the relation to AL122023.1-miR-26a/30d/30e axis

**Elena D. Wilhelm**
University Hospital Essen
**Marc Wiesehöfer**
University Hospital Essen
**Jaroslaw Thomas Dankert**
University Hospital Essen
**Sven Wach**
University Hospital Erlangen
**Mathias Wagner**
University Hospital Saarland
**Martin Spahn**
Lindenhofspital Bern
**Marianna Kruithof de Julio**
Bern University Hospital
**Gunther Wennemuth** ( gunther.wennemuth@uk-essen.de )
University Hospital Essen

**Research Article**

**Keywords:** Prostate cancer, LNCaP, neuroendocrine cells, xCT, AL122023.1, lncRNA, miR-26, miR-30

**Posted Date:** September 15th, 2023

**DOI:** https://doi.org/10.21203/rs.3.rs-3344743/v1

## Abstract

# Purpose

Prostate cancer is the second most common type of cancer in male worldwide. Stromal-epithelial interaction is thought to have a major impact on cancer development and progression. Interaction via soluble factors previously revealed a reduction in the expression of *xCT* and *AL122023.1* in prostate carcinoma cells LNCaP after seven days of co-culture with stromal primary p21 cells. Furthermore, xCT is known to be a putative target for miR-26a, miR-30d and miR-30e which in turn potentially interact with the lncRNA AL122023.1.

# Methods

We validated the repression of *xCT* and *AL122023.1* at RNA level by quantitative real-time PCR and at protein level by Western Blotting. The lncRNA-miRNA-interaction was analyzed by luciferase reporter assays whereas the localization and distribution of xCT in prostate tissue of different developmental stages was evaluated by immunostaining.

# Results

The interaction between AL122023.1 and miR-26a/-30d/-30e was verified and further investigated at protein level regarding xCT. An indirect inhibitory effect of AL122023.1 on the xCT expression could be shown, but miR-26a/-30d/-30e caused no inhibition. Moreover, immunostaining displayed a precise xCT expression in neuroendocrine cells ranging from fetal, healthy juvenile and adult prostate tissue to benign prostatic hyperplasia and finally advanced prostate cancer.

# Conclusion

This study explores the relevance and function of xCT and AL122023.1 in the prostate and exposes xCT as a potential marker or therapeutic target in high-risk prostate cancer.

## 1 Introduction

Most commonly, prostate adenocarcinoma is a malignant transformation of glandular epithelial cells. According to Globocan 2020, prostate cancer (PCa) is the second most common cancer in men worldwide [1]. Although there are numerous treatment options with curative intent for the localized, organ-confined stage, more than 370,000 people still suffer from death due to PCa each year. Still, there is a lot to learn about this heterogenous cancer type regarding development and progression.

From a histological view, the prostate consists of epithelial and stromal cells that interact closely. Prostatic glands are mainly composed of luminal secreting epithelial cells, which pinch off secretory granules either apically or via exocytosis into the glandular lumen (apo- or merocrine) [2]. The glandular epithelium also contains basal stem cells, which are crucial for epithelial renewal, and few neuroendocrine cells (NE cells), which secrete various neuropeptides, such as chromogranin A, serotonin, and neuron-specific enolase [3]. In addition, NE cells are distinguished from other cell types by the absence of the androgen receptor [4, 5]. Regarding the histogenesis, Szczyrba and colleagues demonstrated that neuroendocrine cells of the prostate originate from the neural crest [6]. At the present time however, the exact function of prostatic NE cells is not well understood, but they are thought to have a paracrine influence on the growth and differentiation of surrounding prostate cells. The stroma instead is mainly composed of smooth muscle cells and fibroblasts surrounding the prostate glands [7]. Smooth muscle cells contribute to the expulsion of prostatic secretions from the glands through their contractile activity. Besides, fibroblasts synthesize components of the extracellular matrix, such as glycoproteins, proteoglycans, or collagens to form a structural network. In addition, vessels, immune cells, and nerve fibers can be found in the stroma. Further research on the interaction of epithelial and stromal cells will provide an important basis for a deeper understanding of the development and progression of PCa.

We previously published the mRNA expression profile of LNCaP prostate carcinoma cells and stromal p21 cells after co-culture in terms of soluble factors and highlighted *GALNT14* as a prominent induced gene [8]. Here, we furthermore identified and investigated *xCT* (*SLC7A11*) and *AL122023.1* as co-culture specific, repressed genes in LNCaP cells after paracrine interaction with p21 cells for seven days.

AL122023.1 is a long non-coding RNA (lncRNA), whose function is yet unknown. Besides protein-coding genes, the genome contains numerous non-coding RNAs, which are themselves classified into short (smaller than 200 nucleotides) and long (between 200–1000 nucleotides) non-coding RNAs [9, 10]. Especially, lncRNAs are involved in transcriptional, post-transcriptional and translational regulation and are relevant regarding tumor biology. A typical function is the sponging or sequestering of miRNAs, which in turn are potent negative regulators of mRNA translation [11, 12]. According to recent publications, lncRNAs play a role in the development of resistance to therapeutic agents in PCa [13]. In addition, using the bioinformatics prediction tools DIANA and TargetScan, an indirect link of AL122023.1 to xCT via miR-26a, miR-30d and miR-30e is assumed. xCT, also referred to as SLC7A11 (Solute Carrier Family 7 Member 11), together with SLC3A2 (synonyms: 4F2, CD98) forms a membrane-bound, sodium-independent amino acid antiporter [14]. This heterodimer (Xc  -system) exchanges cytosolic glutamate for extracellular cystine [15] to protect cells against oxidative stress and to maintain the redox balance [16]. Furthermore, xCT is functionally involved in the inhibition of ferroptosis [17]. This iron-dependent cell death might have a clinical relevance in terms of new therapeutic approaches in cancer. This study characterizes xCT in human prostate tissue of different developmental stages as well as pathology and elucidates the relation to AL122023.1, miR-26a and miR-30d/e.

# 2 Results

## 2.1. xCT and AL122023.1 as repressed genes after stromal-epithelial interaction

In order to investigate the expression profiles of LNCaP cells after stromal-epithelial interaction via soluble factors, we previously performed RNA sequencing of LNCaP cells from co-culture experiments with stromal p21 cells for one and seven days [8]. *xCT* and *AL122023.1* were among the most profound repressed genes over time and were therefore chosen for further investigation. To verify of the sequencing results, three independent co-culture experiments followed by quantitative real-time PCR (qRT-PCR) were performed (Fig. 1A). Here, LNCaP cells were cultured within a hanging cell culture insert and p21 cells in the well of a culture plate to create a system of stromal-epithelial interaction without direct contact. Since it cannot be excluded that soluble factors are released in a specific orientation (apical or basal of the cell), the cells were also co-cultured in reverse orientation (n = 3). Again, qRT-PCR analyses confirm the repression of *xCT* and *AL122023.1* after co-cultivation. As the lncRNA *AL122023.1* is not translated into a protein, qRT-PCR analysis simultaneously results in a final confirmation of the gene expression change. For the amino acid antiporter xCT, repression was furthermore validated at protein level by Western Blot analyses (n = 3). After seven days of both co-cultures (LNCaP-p21; p21-LNCaP), expression is reduced by 90,3% (LNCaP-p21) and 78% (p21-LNCaP) on average compared to day 1 (Fig. 1B,C).

## 2.2. AL122023.1-miR-26a/30d/30e axis

Among others, lncRNAs are considered to exhibit a function as sponge or scavenger to sequester microRNAs (miRNAs). MiRNAs themselves are about 18–23 nt long, single-stranded, non-coding RNA molecules. The miRNA seed sequence is crucial for binding to their target sequence, usually located within the 3'-untranslated region (3'UTR) of mRNAs. This miRNA-mRNA-interaction typically inhibits target mRNA translation [11, 12]. Consequently, if miRNAs are captured by lncRNAs, they are no longer able to post-transcriptionally regulate their target mRNAs which could thus function either oncogenic or tumor suppressive [18]. Using the databases DIANA and Starbase, miR-26a-5p, miR-30d-5p, miR-30e-5p were identified as putative interaction partners of *AL122023.1*. To test, if the identified miRNAs are able to interact with *AL122023.1*, luciferase reporter gene constructs were used. For this purpose, the entire sequence of *AL122023.1* (530 bp) was cloned downstream the coding region of the firefly luciferase in the pMIR reporter plasmid to set the reporter gene under the regulative control of *AL122023.1*, now acting as a 3’UTR element. Figure 2A illustrates the predicted binding sites and the seed sequences of miR-26a and miR-30d/e, respectively. All miRNAs have one potential binding site in AL122023.1.

Reporter gene plasmids (pMIR, pMIR-AL122023.1, pMIR-mut_AL122023.1) were co-transfected with miRNA expression vectors (pSG5) in HEK293T cells. Interestingly, miR-26a shows a negative regulatory effect even in the absence of the AL122023.1 sequence where it causes a reduction of about 13% in reporter gene activity ($p \leq 0.001$), while miR-30d and miR-30e have no regulative effect on the reporter gene activity in the absence of the AL122023.1 sequence (Fig. 2B). The presence of the AL122023.1 sequence, acting as a 3’UTR element, makes the reporter gene susceptible for a miRNA-mediated negative

regulation. The luciferase activity decreases by an average of 28% ($p \leq 0.001$) for miR-26a, 29% ($p \leq 0.001$) for miR-30d and 31% ($p \leq 0.001$) for miR-30e (Fig. 2C). To test the specificity of this regulation, we deleted 102 bp at the 3' terminus of the AL122023.1 containing all the predicted miRNA binding sites. The resulting pMIR-mut_AL122023.1 reporter gene construct is completely irresponsive for any miRNA-mediated gene regulation (Fig. 2C). This confirms that the binding sites for the three miRNAs in the AL122023.1 lncRNA are functionally active and able to interact with miR-26a, miR-30d and miR-30e.

Furthermore, xCT was identified as a potential target gene of miR-26a, -30d and – 30e using the database TargetScan, and therefore an indirect effect of AL122023.1 on xCT expression was suspected. To test this hypothesis, xCT expression was examined on protein level by Western Blotting after overexpression of the three miRNAs separately and of AL122023.1 in LNCaP cells (Fig. 2D,E). The expression of either miRNA leads to an increase in xCT protein. Overexpression of miR-26a shows an induction of xCT expression by an average of 66%, miR-30d by 31%, and miR-30e by 62% (Fig. 2D). Although we were able to confirm the functional interaction of miRNAs miR-26a, miR-30d and miR-30e with the lncRNA *AL122023.1*, the suggested miRNA sequestering effect does not seem to be the functional basis of xCT overexpression. In contrast, AL122023.1 overexpression increases xCT expression by an average of 15% (Fig. 2E).

Despite the mode of regulation of xCT expression remains to be elucidated, we could demonstrate a negative regulatory effect, caused by co-cultivation of tumor cells with p21 primary stroma cells. This in fact could render tumor cells more susceptible to cell death caused by oxidative stress. Therefore, we next investigated the expression of xCT in primary tissues at different developmental and malignant stages.

## 2.3. xCT expression in non-malignant prostate tissue

Regarding the localization and distribution in prostate tissue, xCT expression was not only immunohistochemically investigated in benign or malignant prostate tissue, but also in healthy prostate tissue of different developmental stages. As fetal prostate tissue exhibits a variable appearance of glands, for example not yet canalized glands, reference staining with the epithelial marker cytokeratin 7 was performed first (Figure S1). To visualize muscle cells in the stroma, the type 3 intermediate filament desmin was additionally detected before examining xCT (Figure S1).

In five of eight samples, xCT staining is rather weak or barely present in epithelial cells (gestation week: 12; 14.5; 17.1; 18.2; 21.5, the latter representatively depicted in Fig. 3A,E,I). One sample shows a moderate staining of the glandular epithelium (gestation week 14.6). In two cases, distinct strongly xCT-positive cells are detected basally in the epithelium (gestation week: 18; 21.5). In the stroma, xCT-positive cells are mostly detected in marginal areas (Fig. 3I).

To investigate an age-dependent expression of xCT, healthy, juvenile, or adult tissue was stained. For this purpose, specimens from males of different ages (gestation week 21.5, 9 months, 17 years, and 74 years) are representatively demonstrated (Fig. 3). Conspicuously, single strongly xCT-positive cells are present in the glandular epithelium independent of the age (Fig. 3B-D). These cells are mostly located basally and

have a rather small cell size compared to adjacent epithelial cells. Concerning the stroma, it is noticeable that certain cells weakly express xCT (Fig. 3F-H). However, the cell type has not been further identified. Furthermore, present skeletal muscle as well as perikarya of neurons are markedly xCT-positive (Fig. 3J-L, S2). Finally, endothelial cells of some blood vessels show a weak xCT expression. The *tunica media* appears more xCT-positive only in larger vessels. Overall, no age-related increase or decrease of xCT-positive cells in the epithelium or stroma can be detected.

## 2.4. xCT expression in benign prostatic hyperplasia (BPH) and rhabdomyosarcoma of the prostate

BPH is a benign enlargement of the prostate gland whereas the rhabdomyosarcoma is a malignant neoplasm originating from muscle cells. Both were used to study xCT expression in pathologically altered tissue in addition to PCa.

In BPH tissue (n = 5; age: 60, 66, 70, 76, 86), the glandular epithelium is mainly xCT-negative, with isolated strongly xCT-positive cells (Fig. 4A-B). In general, they are located basally and have a small cell size. The stroma shows a heterogeneous staining pattern. Apparently, only one specific cell type seems to be xCT-positive, which occurs irregularly distributed (Fig. 4C). In skeletal muscle distant from glands and in perikarya of neurons, xCT is detectable, whereas the endothelium of small blood vessels is rather weakly xCT-positive (Fig. 4D, S2). A more concise staining is only visible in larger vessels with a *tunica media*. In summary, xCT expression in BPH equals the one in healthy juvenile and adult tissue.

To investigate the embryonal rhabdomyosarcoma (ERMS, n = 1) of the prostate of a 17-year-old male, the marker protein desmin was visualized first to detect the tumor cells. Additionally, staining with anti-CD68-antibodies was previously performed to distinguish tumor cells from macrophages [8]. Furthermore, a cytokeratin 7 reference staining was applied to test whether intact glandular epithelium is present [8]. Adjacent normal prostate tissue shows the typical staining of distinct cells within the glandular epithelium (Fig. 4E). The tumor lacks intact glandular tissue, but contains numerous desmin-positive cells, which also clearly express xCT (Fig. 4F).

## 2.5. xCT expression in prostate carcinoma

To investigate the presence of xCT in PCa tissue, the general expression on RNA level was determined by qRT-PCR. Six cryopreserved PCa samples with a Gleason score < 8 (< GS8) and five with a Gleason score ≥ 8 (GS ≥ 8) as well as the respective adjacent normal tissue were available for this study. For the comparison of normal and PCa tissue, xCT expression in normal tissue was expressed as a distribution around the mean first and then related to the expression in PCa. While *xCT* expression in normal tissue varies greatly between repressed and induced, there is an average induction of *xCT* expression in PCa compared to normal tissue (*, $p \leq 0.05$) (Fig. 5A). In addition, a rising xCT expression with increasing Gleason score can be observed. The xCT expression doubles comparing samples < GS8 to ≥ GS8 (average $\log_2 \approx 1$ in < GS8 and $\log_2 \approx 2.2$ in ≥ GS8). Last, the overall induction of *xCT* in PCa is

confirmed by results from the database GEPIA (Fig. 5A). In total, an induction and a rising expression of xCT with increasing Gleason score can be shown. Similar results are obtained for *AL122023.1* expression in those samples. The comparison of PCa and tumor-adjacent normal tissue reveals an average 1.7-fold increase ($\log_2 \approx 0.8$ in ≥ GS8, not significant) in *AL122023.1* expression with increasing Gleason score (Fig. 5B). Results from the database GEPIA confirm the induction of AL122023.1 in PCa (Fig. 5B).

Next, subsequent immunohistochemical staining of PCa tissue revealed the localization of xCT. For this purpose, four tissue microarrays (TMAs) were used containing a total of 196 prostate punch biopsies with different Gleason scores from 174 individual patients aged 47–78 years. An overview of the evaluated samples is shown in Table 1. When two samples per patient were available, then both were included in the analysis if they differed in Gleason score, which was the case for 22 patients.

Table 1
Overview of evaluated samples for xCT expression and number of patients depending on Gleason score.

| Gleason score | Sample size | Number of patients |
|---|---|---|
| **3 + 3 (6)** | 41 | 35 |
| **3 + 4 and 4 + 3 (7)** | 56 | 50 |
| **4 + 4 (8)** | 40 | 35 |
| **≥ 4 + 5 (≥ 9)** | 59 | 54 |

First, the general presence or absence of xCT-positive cells was determined (Table 2, Fig. 5C). Cells with a precise xCT signal are detected in 63 samples, while 133 are negative. As already identified for healthy prostate tissue (fetal, juvenile, adult) and BPH, anti-xCT staining in PCa tissue also focuses mainly on single cells in the glandular epithelium. Regarding samples with a Gleason score of 6, only a few single cells are xCT-positive. This number of xCT-positive cells per sample as well as samples even displaying stained cells slightly increases for Gleason score 7. Conspicuously, from a Gleason score of 8, a growing number of samples are xCT-negative. However, if xCT is detected, the number of xCT-positive cells within one sample increases significantly. Overall, there seems to be an accumulation of xCT-positive cells in some specific PCa samples with increasing Gleason score.

Table 2
Overview of presence or absence of xCT expression in tumor cells depending on the Gleason score.

| Gleason score | present | absent |
|---|---|---|
| **3 + 3 (6)** | 14 (34%) | 27 (66%) |
| **3 + 4 and 4 + 3 (7)** | 28 (50%) | 28 (50%) |
| **4 + 4 (8)** | 11 (28%) | 29 (72%) |
| **≥ 4 + 5 (≥ 9)** | 10 (17%) | 49 (83%) |

The presence of xCT was also examined in the adjacent stroma. For this purpose, the stroma was classified into four categories: no staining, weak, moderate, or strong staining. How these modes were visually categorized is shown in Fig. 5D. Corresponding results for the number of samples per expression intensity are listed in Table 3.

Table 3
Overview of expression intensity (none, weak, moderate, strong) of xCT in tumor cells depending on the Gleason score.

| | Expression intensity (sample size) | | | |
|---|---|---|---|---|
| **Gleason score** | **None** | **weak** | **moderate** | **strong** |
| **3 + 3 (6)** | 16 | 17 | 8 | / |
| **3 + 4 und 4 + 3 (7)** | 19 | 28 | 7 | 2 |
| **4 + 4 (8)** | 25 | 13 | 2 | / |
| **≥ 4 + 5 (≥ 9)** | 38 | 20 | 1 | / |

A similar expression pattern and intensity in the stroma is identified as shown for healthy prostate tissue and BPH. In general, either no or a very weak xCT expression is detected across Gleason scores in stromal cells. Few samples display a moderate staining and for only two samples with Gleason score 7 even a strong staining is detected. Moreover, there is no correlation between the tumor-adjacent stroma and the presence or amount of tumor cells, whether xCT-positive or -negative.

Since only single cells in the glandular epithelium repeatedly appeared xCT-positive in both healthy juvenile and adult prostate tissue as well as in BPH and partly in PCa tissue, we hypothesized that these represent neuroendocrine cells. Therefore, a healthy prostate tissue sample from a 64-year-old man, which showed comparatively many cells with distinct xCT expression, was selected for double-immunofluorescence staining for the neuroendocrine marker chromogranin A (CgA) (Fig. 6A).

The double staining of xCT and CgA reveals an evident colocalization and therefore confirms the hypothesis that neuroendocrine cells in the glandular epithelium of the prostate express xCT. Next, it was

investigated whether xCT-positive cells in PCa also represent neuroendocrine cells. For this purpose, TMAs stained with anti-xCT antibodies were compared to TMAs prior stained with anti-CgA antibody by the University of Bern (Fig. 6B). Morphological differences in PCa sample result from different sectioning levels in the tissue cylinder. The optical differences are the result of different scanning methods. Again, the anti-xCT staining pattern closely resembles the anti-CgA staining, suggesting that cells coexpress xCT and CgA. To finally verify whether neuroendocrine-like tumor cells in PCa also show the same expression pattern after androgen deprivation therapy, five rare samples were analyzed. A representative staining result is shown in Fig. 6C. For neuroendocrine-differentiated prostate tumors, we demonstrate that xCT is exclusively detected in CgA-positive cells. In summary, these results show for the first time that neuroendocrine cells in healthy and pathological prostate tissue as well as transdifferentiated neuroendocrine-like cells express xCT.

# 3 Discussion

We previously published results of a deregulated mRNA expression in LNCaP cells after interaction with stromal p21 cells via soluble factors [8]. Here, a repression of *xCT* and *AL122023.1* after seven days of co-culture was verified by qRT-PCR in three independent experiments. Moreover, validation of repressed expression of *xCT* and *AL122023.1* after reverse co-cultivation argues for apical and basolateral secretion of soluble factors. Finally, Western Blot analysis also confirmed the repression of xCT at the protein level. In this context it is worth noting that there is still an ongoing debate about which result to expect in a western blot hybridization for xCT. Several public databases (NCBI, Uniprot) predict a molecular weight of around 55 kDa for the 501 amino acid protein. Indeed, Chen et al. [19] identified a xCT band at around 57 kDa, whereas Liefferinge and colleagues showed that the actual size must be closer to 35 kDa [20]. Therefore, the characteristics of antibodies used in this study was tested by overexpression of xCT in cells, protein extraction and finally analysis by Western Blotting (Figure S3). xCT (1506 bp) cloned in pcDNA3.1 vector was obtained by Vectorbuilder and the sequence double-checked by an commercial vendor (LGC Genomics, Berlin, Germany). For three different antibodies (PA1-16893, Invitrogen; #711589 (clone 3HCLC), Invitrogen; 12691S (clone D2M7A), Cell Signaling), xCT could be uniquely identified at the level of 35 kDa.

As the RNA sequencing data was repeatedly confirmed by different experiments, xCT and AL122023.1 were further investigated. Here, they turned out to be linked by miR-26a, miR-30d and miR-30e. In this regard, Wach and colleagues, like our own results, showed a direct correlation between induced expression of miR-26b and corresponding induction of xCT in collecting duct renal cell carcinoma [21]. Studies on the interaction of miR-26b or -30b and xCT already confirmed the functionality of the binding sites via luciferase reporter assays [22–24]. Since miR-26a, -30d and – 30e belong to the same miRNA family, they share the same core seed sequence that is crucial for binding. Therefore, they are expected to bind to the 3'UTR of xCT and thus inhibit xCT expression. However, the results of our Western Blot analyses showed an average induction of xCT expression, when either of the three miRNAs is ectopically expressed. According to the DIANA tool TarBase v.8, those miRNAs have a variety of potential target genes. Therefore, the elevated expression of xCT might be caused by repressing other target proteins and

enhancing translation. Moreover, it is conceivable that only a combination of miRNAs could provide an inhibition of xCT expression in prostate cancer cells. In addition, lncRNAs are becoming increasingly important in terms of their miRNA regulatory function. For example, the lncRNA TUG1 has been shown to play a role in PCa development by regulating the function of miR-26a [25]. Congruously, this work identified the lncRNA AL122023.1 as a potential interacting partner for the miR-26 and miR-30 families. A repressed expression of AL122023.1 would result in an elevated concentration of miRNA molecules that, by a yet unknown pathway, could inhibit the expression of *xCT*. Since *xCT* is also repressed after seven days of co-culture in LNCaP cells, there might be a causal relationship. Luciferase reporter assays confirmed the unambiguous binding of miR-26a, -30d and – 30e to the predicted binding sites within *AL122023.1*. Furthermore, we determined the indirect effect of AL122023.1 on the expression of xCT in LNCaP cells by Western Blot analysis. The results showed a corresponding increase in xCT expression by 15% on average. This relatively weak induction of xCT could either be due to a low endogenous miRNA level or due to the fact that lncRNAs only scavenges miRNAs for a certain period of time but do not degrade them. Thus, miRNAs could possibly lead to the inhibition of xCT expression again after a time delay. Corresponding kinetics would provide new insights. We also showed an induced *AL122023.1* expression in PCa with increasing Gleason score. Consequently, *xCT* expression also increased, again suggesting a causal relationship between AL122023.1 and xCT.

Immunohistochemical staining was intended to provide an overview of xCT expression in prostate tissue of different origins. During prostate development, only very few basally located cells within glandular epithelium express xCT. The stroma predominantly shows no or at most very weak xCT expression, although there are also marginal areas with clearly stained cells. The latter are not further characterized though. In general, the function of xCT during embryogenesis has been poorly investigated. xCT knockout mice (xCT-/-) of both sexes showed no lethality and normal fertility [26]. Only blood plasma showed an increased cystine concentration and a decreased intracellular GSH concentration. Interestingly, a comparable concentration of intracellular cystine in embryonic fibroblasts was found in wild-type and KO mice. These results suggest that the cell has compensatory mechanisms to provide cystine and may also thus protect the cell from ferroptosis. In this regard, transsulfuration of methionine or even ASC transporters (ASCT1/ SLC1A4, ASCT2/ SLC1A5) represent a crucial alternative [27]. Furthermore, an age-related expression change was investigated using healthy tissue of male differing in age (9 month to 84 years). Analysis revealed a distinct staining of individual cells in the glandular epithelium, which appeared to be neuroendocrine cells. The stroma, like in fetal prostate tissue, was largely xCT-negative except for single cells in specific areas. Overall, there was no age-related increase or decrease of xCT-positive cells in the glandular epithelium or in cells of the stroma. Additionally, there was a clear staining of adjacent skeletal muscle. This suggests that xCT-positive cells in the stroma can also be muscular cells. Conveniently, Huang and colleagues found that there is a relationship between sarcopenia, the age-related decrease in muscle mass and strength, and ferroptosis [28]. They attributed accumulation of iron in muscle to p53-related repression of xCT. Next, the investigation of xCT expression in benign prostatic hyperplasia (BPH) featured same characteristics as healthy tissue. Thus, it can be concluded that xCT does not play a specific role in BPH.

The correlation of xCT deregulation and PCa is currently gaining interest. Various therapeutics are described for a targeted induction of ferroptosis in castration-resistant PCa, already. These include Flubendazole [29], Sulfasalazine [30, 31], Sorafenib [32], Erastin, and RSL-3 [33]. Complementary, we detected an average induction of xCT expression in PCa with increasing Gleason score at RNA level and also at protein level. With increasing Gleason score, an accumulation of xCT-positive cells within a sample was more likely. However, xCT was detected in fewer samples overall above a Gleason score of 8. Additionally, patient-related data did not indicate corresponding factors, such as PSA concentration or therapeutic intervention (data not shown). However, this study demonstrated that xCT-positive tumor cells were neuroendocrine or at least neuroendocrine-like cells as they also expressed the neuroendocrine marker protein chromogranin A [34, 35]. Therefore, xCT might serve as potential marker protein for advanced PCa. Besides, these results also highlight the relevance for therapeutic interventions, as androgen-resistant tumor cells can apparently escape ferroptosis by increased expression of xCT. In future, effective treatments for advanced PCa could be achieved by targeting ferroptosis in tumor cells. According to a recent study, the combination of the androgen receptor antagonist enzalutamide and the ferroptosis-inducing substances erastin or RSL3 has an inhibitory effect on prostate tumor growth in vivo [33]. Also, parallel administration of sulfalazine together with the vasodilator oxyfedrine made tumor cells more susceptible to ferroptosis [36].

In conclusion, this work shows that androgen-sensitive prostate carcinoma cells exhibit reduced xCT expression in the presence of stromal cells *in vitro*, while on the other hand xCT is increasingly expressed in androgen-resistant, neuroendocrine-like cells in PCa tissue. Accordingly, this work shows the relevance of the tumor microenvironment and that the study of cell-cell communication is necessary to better understand the development and progression of PCa. Finally, xCT as an important regulator of ferroptosis generates numerous new research approaches associated with a high clinical relevance. xCT may serve as a novel neuroendocrine marker and is also progressively gaining importance as a therapeutic target in prostate cancer.

# 4 Materials and Methods

# 4.1. Cell lines and transfections

HEK293T cells (*Human Embryonic Kidney* 293 cells; RRID:CVCL_0063; American Type Culture Collection ATCC/LGC Standards GmbH, Wesel, Germany) were grown in DMEM (*Dulbecco's Modified Eagle Medium*; Thermo Fisher Scientific, Schwerte, Germany) supplemented with 10% heat-inactivated fetal bovine serum (Life Technologies (Gibco), Thermo Fisher Scientific, Oberhausen, Germany), 100 U/ml penicillin and 100 µg/ml streptomycin. LNCaP cells (*Lymph Node Carcinoma of Prostate* cells; RRID:CVCL_0395; Sigma-Aldrich, Hamburg, Germany) were cultivated in RPMI 1640 medium (*Roswell Park Memorial Institute* 1640; Thermo Fisher Scientific, Oberhausen, Germany) with same supplements and additionally 1 mM pyruvate (Thermo Fisher Scientific, Schwerte, Germany). Cells were last authenticated by ATCC, performing STR Profiling following ISO 9001:2008 and ISO/IEC 17025:2005 quality standards. Exclusion

of Mycoplasma infection was tested as previously described [8]. Cultivation of primary p21 cells as well as their co-cultivation with LNCaP cells was performed as described priorly [8].

In general, $5x10^5$ LNCaP cells or $6x10^5$ HEK293T cells were seeded into 6-well plates, transfected with 2 µg expression plasmid DNA using jetPRIME transfection reagent (Polyplus transfection, Sélestat, France) on the following day to finally isolate RNA or protein after further 48 h. As transfection control, GFP (transfection with pAcGFP-C1 expression plasmid) was detected by microscope *Eclipse Ni* (Nikon, Amsterdam. Netherlands).

# 4.2. Human prostate specimens

Same samples were used as described previously [8]. The Institute of General and Special Pathology at Saarland University Hospital in Homburg provided fetal tissue (n = 2), normal tissue of different age (n = 9), BPH (n = 5) and rhabdomyosarcoma (n = 1) (ethics approval University of Duisburg-Essen 18-7959-BO). Additional fetal tissue (n = 6) was obtained from Dr. Laurence Baskin at the Department of Urology, University of California, San Francisco (UCSF) (local ethics approval plus inclusion in 18-7959-BO). Prostate carcinoma tissue was provided by the following collaborations: Tissue biobank of the Comprehensive Cancer Center (CCC-ER EMN) of the University Hospital Erlangen in cooperation with Prof. Dr. Helge Taubert and Dr. Sven Wach (project no. 2019 – 112; n = 11 cryoconserved); Department of Urology at the Community Hospital Karlsruhe or EMPaCT tumor bank (European Multicenter Prostate Cancer Clinical and Translational Research Group) in cooperation with Prof. Dr. Martin Spahn, PD Dr. phil. Marianna Kruithof-de Julio and Dr. phil. Eugenio Zoni (n = 203 of N = 180 paraffin-embedded) (ethics approval KEK Bern No. 128/2015) [37]. Tissue microarrays (TMAs) were generated by multiple tumor samples derived from the index lesion including more differentiated areas of each tumor as well as matched lymph node metastasis from previously untreated patients. The expression of several tumor relevant genes (e.g. AR, PTEN, p53, MLH1, CD44, ALDH1, chromogranin A, and synaptophysin) and the TMPRSS2-ERG gene fusion was also analyzed on TMAs [38, 39].

Pathological tissue was reviewed by local pathologists at the respective sites.

# 4.3. RNA isolation

Total RNA was isolated from cell lines using the miRNeasy Mini Kit (Qiagen, Hilden, Germany) according to the manufacturer's instruction. The BioPhotometer (Eppendorf, Hamburg, Germany) was used to determine the RNA concentration and quality.

# 4.4. cDNA synthesis and quantitative real-time PCR

cDNA synthesis of mRNA and analysis of the relative gene expression was realized as previously described [8]. Besides, miRNAs were transcribed into cDNA using miRCURY LNA RT Kit (Qiagen, Hilden, Germany) according to manufacturer's instruction. QRT- PCR was performed using the miRCURY LNA SYBR® Green PCR Kit (Qiagen, Hilden, Germany) according to the manufacturer's protocol and the real-time PCR detection system qTower$^3$G (Analytic Jena, Jena, Germany). To quantify the target gene

expression, 5S rRNA served as reference gene using the ΔΔCt method. Duplicates and Non Template Controls (NTC) were included in every experiment. The thermal cycling conditions for miRNAs were as follows: 95°C for 2 min followed by 40 cycles of 95°C for 10 sec and 56°C for 60 sec. To ensure purity and specificity of PCR, a melting curve analysis was performed. Table S1 lists all oligonucleotide sequences for mRNA and miRNA detection.

# 4.5. Non-radioactive Northern Blot

At least 10 µg total RNA were separated on Mini-PROTEAN® TBE-Urea Precast gels or on 12% denaturing urea PAGE (SequaGel-UreaGel System; National Diagnostics, Beutelsbach, Germany). To ensure a comparable loading, gels were immersed in GelRed (1:20000 in TBE) and RNA detected by UV light with the ChemiDoc Touch Imaging System (Bio-Rad, Hercules, CA USA). RNA was then transferred to the nylon membrane Amersham Hybond-N+ (GE Healthcare Life Science, Freiburg, Germany) in a semi-dry transfer cell (BioRad, Munich, Germany; 30 min at 15 V) and chemically cross-linked with the soluble carbodiimide, EDC, for 60 min at 55°C. Hybridization of blots with 5'biotin-labeled antisense probes was performed at 50°C overnight and membranes were then washed twice with 5X SSC/ 0.1% SDS and 1X SSC/ 0.1% SDS for 15 min at 50°C. For detection of hybridized probes, HRP conjugated Streptavidin (R&D Systems, Minneapolis, MN USA, 1:1000) was incubated for 1 h and detected by the Clarity™ Western ECL Substrate according to the manufacturer's specifications. Target miRNA were finally visualized by the ChemiDoc Touch Imaging System (Bio-Rad, Hercules, CA USA). Table S2 contains the probe sequences.

# 4.6. Target prediction

TargetScan (release 8.0; http://www.targetscan.org/) was used for miRNA target prediction. Databases DIANA (release lncBase v.3; https://diana.e-ce.uth.gr/lncbasev3/interactions) and Starbase (release v2.0; https://starbase.sysu.edu.cn) helped to predict lncRNA-miRNA-interaction.

# 4.7. Plasmids

All oligonucleotide sequences were amplified from human genomic DNA. MiR-26a (nucleotides 37969254–37969610 of chromosome 3), miR-30d (nucleotides 134804658–134805143 of chromosome 8) and miR-30e (nucleotides 40754221–40754542 of chromosome 1) were inserted into the pSG5 expression vector (Agilent technologies, Ratingen, Germany). AL122023.1 (amplicon size: 530 bp, nucleotides 93334528–93335057 of forward strand on chromosome 14 (GRCh38), Ensembl number: ENSG00000278396) was inserted into the pcDNA3.1(+) expression vector (Thermo Fisher Scientific, Oberhausen, Germany). QRT-PCR and Northern Blotting verified overexpression in HEK293T or LNCaP cells (Figure S4).

For luciferase reporter assays, the AL122023.1 sequence was inserted into the modified pMIR-RNL-TK reporter vector (Thermo Fisher Scientific, Oberhausen, Germany) as described elsewhere [40]. The reporter plasmid expresses the firefly luciferase mRNA including the sequence of interest and constitutively expresses the renilla luciferase as an internal normalization control. A shortage of the AL122023.1

fragment removed potential binding sites for miRNAs. Table S3 depicts all oligonucleotide sequences for molecular cloning.

## 4.8. Dual-Luciferase reporter assay

To analyze the lncRNA-miRNA-interaction, $2x10^5$ HEK293T cells were seeded into a 24-well plate. Cells were then transfected with 0.2 µg pMIR-RNL-TK reporter plasmid (containing lncRNA) and 0.8 µg pSG5 effector plasmid (containing miRNA) using JetPrime (Polyplus transfection, Illkirch, France) on the following day. After an incubation for 48 h, cells were prepared for the dual luciferase reporter assay system (Promega, Mannheim, Germany) according to the manufacturer's instruction. Detection of luminescence was exhibit using the luminometer Lucetta (Lonza, Basel, Schweiz). To quantify the relative luciferase activity, the determined light emission of the firefly luciferase was normalized with that of the constitutively expressed renilla luciferase. Values to be compared were finally correlated.

## 4.9. Protein extraction and Western Blotting

$5x10^5$ LNCaP cells or $6x10^5$ HEK293T cells were seeded into a 6-well plate and after 48 h, transfected with 2 µg expression plasmid DNA using jetPRIME transfection reagent (Polyplus transfection, Illkirch, France). After two further days, protein lysates were extracted with 90 µl RIPA buffer (5 M NaCl, 0,5 M EDTA (pH 8,0), 1 M Tris (pH 8,0), 10% Natriumdesoxycholat, 10% SDS plus protease/phosphatase inhibitor). Protein lysates were supplemented with denaturating gel loading buffer (4X Laemmli buffer: 8% SDS, 20% 3-Mercapto-1,2-propandiol, 40% Glycerol, 0,008% Bromphenolblau, 0,25 M Tris HCl) and separated by electrophoresis on 8–16% *Mini- PROTEAN TGX Precast* gels or on 12% gels using the *TGX Stain-free FastCast Acrylamide Kit* (Bio-Rad, Hercules, CA USA). Separated proteins were transferred by semi-dry blotting on the *Trans-Blot Turbo* PVDF membrane using the *Trans-Blot Turbo Transfer System* (Bio-Rad, Hercules, CA USA).

For immune detection, the following primary antibodies were incubated over night: Rabbit anti-SLC7A11/xCT (12691S, clone D2M7A, Cell Signaling, Leiden, Netherlands; 1:1000 in 5% BSA) and rabbit anti-GAPDH (AB181602, Abcam, Cambridge, UK; 1:1000 in 2% skim milk). A HRP-conjugated goat anti-rabbit IgG (111-035-144, Jackson Immuno-Research, PA, USA; 1:10.000 in corresponding blocking solution) was incubated for 1 h. Finally, the Clarity Western ECL Substrate was used to detect proteins according to the manufacturer's specifications and detected by the ChemiDoc Touch Imaging System (Bio-Rad, Hercules, CA USA).

## 4.5. Immunohistochemical and immunofluorescence staining

Immunohistochemical and immunofluorescence staining was performed as previously described in detail [8]. Following primary antibodies were used: rabbit anti-SLC7A11/xCT (5 µg, PA-16893, Thermo Fisher Scientific, Oberhausen, Germany) and mouse anti-chromogranin A (1:100, ab715, Abcam, Cambridge, UK). A negative isotype control (IgG fraction of non-immunized rabbits or mouse anti-rat-CEACAM1 (IgG κ)) and a positive tissue control complemented each staining (Figure S1).

## 4.6. Statistical Analyses

Quantification of Western Blots was performed by ImageJ 1.52a (National Institute of Health, Bethesda, MD, USA). Data of qRT-PCR and luciferase reporter assays were analyzed and visualized using SigmaPlot 13 (Systat, Erkrath, Germany) or GraphPad Prism 9 (GraphPad Software, San Diego, CA USA). Differences between two sets of data were statistically evaluated with Student's unpaired, two-tailed t-test or Mann-Whitney U-test. Probability values (p-values) $< 0.05$ were considered as significant and indicated with $*$, $**$ $p < 0.01$, $***$ $p < 0.001$. All results are represented as mean ± standard deviation from at least three independent measurements. To perform prostate cancer/normal differential expression analysis, the database GEPIA (Gene Expression Profiling Interactive Analysis) was used with default adjustments [41].

# Declarations

Conflict of Interest

*The authors declare that the research was conducted in the absence of any commercial or financial relationships that could be construed as a potential conflict of interest*.

Author Contributions

Conceptualization, E.D.W.; methodology, E.D.W.; validation, E.D.W. and M.Wa.; formal analysis, E.D.W.; investigation, E.D.W. and M.W.; resources, M.Wa., M.S., M.K. and S.W.; data curation, E.D.W.; writing—original draft preparation, E.D.W.; writing—review and editing, J.T.D., M.W., G.W., S.W.; visualization, E.D.W.; supervision, E.D.W., J.T.D. and G.W.; project administration, E.D.W., J.T.D. and G.W.; funding acquisition, G.W. All authors have read and agreed to the published version of the manuscript.

Funding

This research received no external funding.

Institutional Review Board Statement

The study was conducted according to the guidelines of the Declaration of Helsinki, approved by the Kantonale Ethikkomission (KEK) Bern (128/2015) and the ethics committee of the University of Duisburg-Essen (Ref: 18-7959-BO).

Acknowledgments

We thank Natalie Knipp and Christian von Massow for expert technical assistance and Bernhard B. Singer (University Hospital Essen, Department of Anatomy) for providing IgG fraction of non-immunized rabbits and mouse anti-rat-CEACAM1 (IgG κ). We additionally acknowledge our cooperating partners for the acquisition of the prostate tissue: Dr. med. Fidelis Flockerzi, Dr. Iulia Vasilaki and Johannes Hohneck

(University Hospital Saarland, Department of General and Special Pathology) as well as Dr. Laurence Baskin (University of California, San Francisco, Department of Urology).

Supplementary Material

Data Availability Statement

All data generated or analyzed in this study are included in this article including the supplementary materials.

# References


1. H. Sung, J. Ferlay, R.L. Siegel, M. Laversanne, I. Soerjomataram, A. Jemal, F. Bray, CA Cancer J Clin. **71**, 209–249 (2021). 10.3322/caac.21660
2. N.J. Fullwood, A.J. Lawlor, P.L. Martin-Hirsch, S.S. Matanhelia, F.L. Martin, Sci. Rep. **9**, 4582 (2019). 10.1038/s41598-019-40820-2
3. M.A. Noordzij, G.J. van Steenbrugge, T.H. van der Kwast, F.H. Schroder, Urol. Res. **22**, 333–341 (1995). 10.1007/BF00296871
4. J.L. Krijnen, P.J. Janssen, J.A. Ruizeveld de Winter, H. van Krimpen, F.H. Schroder, and T.H. van der Kwast, Histochemistry. **100**, 393–398 (1993). 10.1007/BF00268938
5. H. Bonkhoff, U. Stein, K. Remberger, Virchows Arch. A Pathol. Anat. Histopathol. **423**, 291–294 (1993). 10.1007/BF01606893
6. J. Szczyrba, A. Niesen, M. Wagner, P.M. Wandernoth, G. Aumuller, G. Wennemuth, J. Biol. Chem. **292**, 2021–2031 (2017). 10.1074/jbc.M116.755082
7. R. Toivanen, M.M. Shen, Development. **144**, 1382–1398 (2017). 10.1242/dev.148270
8. M.W.E.D. Czyrnik, J.T. Dankert, S. Wach, M. Wagner, M. Spahn, M. Kruithof-de, Julio, G. Wennemuth, Front. Oncol. **13** (2023). 10.3389/fonc.2023.1212585
9. F.J. Slack, A.M. Chinnaiyan, Cell. **179**, 1033–1055 (2019). 10.1016/j.cell.2019.10.017
10. J.S. Mattick, I.V. Makunin, Hum. Mol. Genet. 15 Spec. No. 1R17–29 (2006). 10.1093/hmg/ddl046
11. D.P. Bartel, Cell. **136**, 215–233 (2009). 10.1016/j.cell.2009.01.002
12. B.P. Lewis, C.B. Burge, D.P. Bartel, Cell. **120**, 15–20 (2005). 10.1016/j.cell.2004.12.035
13. L. Ding, R. Wang, D. Shen, S. Cheng, H. Wang, Z. Lu, Q. Zheng, L. Wang, L. Xia, G. Li, Cell. Death Dis. **12**, 590 (2021). 10.1038/s41419-021-03854-x
14. H. Sato, M. Tamba, T. Ishii, S. Bannai, J. Biol. Chem. **274**, 11455–11458 (1999). 10.1074/jbc.274.17.11455
15. S. Bannai, J. Biol. Chem. **261**, 2256–2263 (1986)
16. S.C. Lu, Mol. Aspects Med. **30**, 42–59 (2009). 10.1016/j.mam.2008.05.005

17. W.S. Yang, R. SriRamaratnam, M.E. Welsch, K. Shimada, R. Skouta, V.S. Viswanathan, J.H. Cheah, P.A. Clemons, A.F. Shamji, C.B. Clish, L.M. Brown, A.W. Girotti, V.W. Cornish, S.L. Schreiber, B.R. Stockwell, Cell. **156**, 317–331 (2014). 10.1016/j.cell.2013.12.010
18. S. Lin, R.I. Gregory, Nat. Rev. Cancer. **15**, 321–333 (2015). 10.1038/nrc3932
19. D. Chen, Z. Fan, M. Rauh, M. Buchfelder, I.Y. Eyupoglu, N. Savaskan, Oncogene. **36**, 5593–5608 (2017). 10.1038/onc.2017.146
20. J. Van Liefferinge, E. Bentea, T. Demuyser, G. Albertini, V. Follin-Arbelet, S. Holmseth, E. Merckx, H. Sato, J.L. Aerts, I. Smolders, L. Arckens, N.C. Danbolt, A. Massie, J. Comp. Neurol. **524**, 1015–1032 (2016). 10.1002/cne.23889
21. S. Wach, H. Taubert, K. Weigelt, N. Hase, M. Kohn, D. Misiak, S. Huttelmaier, C.G. Stohr, A. Kahlmeyer, F. Haller, J. Vera, A. Hartmann, B. Wullich, X. Lai, Cancers (Basel). **12** (2019). 10.3390/cancers12010064
22. X.X. Liu, X.J. Li, B. Zhang, Y.J. Liang, C.X. Zhou, D.X. Cao, M. He, G.Q. Chen, J.R. He, Q. Zhao, FEBS Lett. **585**, 1363–1367 (2011). 10.1016/j.febslet.2011.04.018
23. J. Du, X.H. Li, F. Liu, W.Q. Li, Z.C. Gong, Y.J. Li, Clin Transl Gastroenterol 11, e00178 (2020) 10.14309/ctg.0000000000000178
24. H. Zhang, Y. He, J.X. Wang, M.H. Chen, J.J. Xu, M.H. Jiang, Y.L. Feng, Y.F. Gu, Redox Biol. **29**, 101402 (2020). 10.1016/j.redox.2019.101402
25. B. Yang, X. Tang, Z. Wang, D. Sun, X. Wei, Y. Ding, Biosci. Rep. **38** (2018). 10.1042/BSR20180677
26. H. Sato, A. Shiiya, M. Kimata, K. Maebara, M. Tamba, Y. Sakakura, N. Makino, F. Sugiyama, K. Yagami, T. Moriguchi, S. Takahashi, S. Bannai, J. Biol. Chem. **280**, 37423–37429 (2005). 10.1074/jbc.M506439200
27. S.L. Cramer, A. Saha, J. Liu, S. Tadi, S. Tiziani, W. Yan, K. Triplett, C. Lamb, S.E. Alters, S. Rowlinson, Y.J. Zhang, M.J. Keating, P. Huang, J. DiGiovanni, G. Georgiou, E. Stone, Nat. Med. **23**, 120–127 (2017). 10.1038/nm.4232
28. Y. Huang, B. Wu, D. Shen, J. Chen, Z. Yu, C. Chen, Int. J. Biol. Sci. **17**, 151–162 (2021). 10.7150/ijbs.53126
29. X. Zhou, L. Zou, W. Chen, T. Yang, J. Luo, K. Wu, F. Shu, X. Tan, Y. Yang, S. Cen, C. Li, X. Mao, Pharmacol. Res. **164**, 105305 (2021). 10.1016/j.phrs.2020.105305
30. D.W. Doxsee, P.W. Gout, T. Kurita, M. Lo, A.R. Buckley, Y. Wang, H. Xue, C.M. Karp, J.C. Cutz, G.R. Cunha, Y.Z. Wang, Prostate. **67**, 162–171 (2007). 10.1002/pros.20508
31. Z. Zheng, G. Luo, X. Shi, Y. Long, W. Shen, Z. Li, X. Zhang, Cell. Oncol. (Dordr). **43**, 95–106 (2020). 10.1007/s13402-019-00474-8
32. E. Lachaier, C. Louandre, C. Godin, Z. Saidak, M. Baert, M. Diouf, B. Chauffert, A. Galmiche, Anticancer Res. **34**, 6417–6422 (2014)
33. A. Ghoochani, E.C. Hsu, M. Aslan, M.A. Rice, H.M. Nguyen, J.D. Brooks, E. Corey, R. Paulmurugan, T. Stoyanova, Cancer Res. **81**, 1583–1594 (2021). 10.1158/0008-5472.CAN-20-3477

34. P.A. Abrahamsson, Endocr. Relat. Cancer. **6**, 503–519 (1999). 10.1677/erc.0.0060503
35. V. Parimi, R. Goyal, K. Poropatich, X.J. Yang, Am. J. Clin. Exp. Urol. **2**, 273–285 (2014)
36. Y. Otsuki, J. Yamasaki, K. Suina, S. Okazaki, N. Koike, H. Saya, O. Nagano, Cancer Sci. **111**, 127–136 (2020). 10.1111/cas.14224
37. M. Spahn, S. Kneitz, C.J. Scholz, N. Stenger, T. Rudiger, P. Strobel, H. Riedmiller, B. Kneitz, Int. J. Cancer. **127**, 394–403 (2010). 10.1002/ijc.24715
38. S. Joniau, A. Briganti, P. Gontero, G. Gandaglia, L. Tosco, S. Fieuws, B. Tombal, G. Marchioro, J. Walz, B. Kneitz, P. Bader, D. Frohneberg, A. Tizzani, M. Graefen, P. van Cangh, R.J. Karnes, F. Montorsi, H. Van Poppel, M. Spahn, European Multicenter Prostate Cancer and G. Translational Research. Eur. Urol. **67**, 157–164 (2015). 10.1016/j.eururo.2014.01.020
39. M. Spahn, A. Briganti, U. Capitanio, B. Kneitz, P. Gontero, J.R. Karnes, M. Schubert, F. Montorsi, C.J. Scholz, P. Bader, H. van Poppel, S. Joniau, European Multicenter Prostate Cancer and G. Translational Research. J. Urol. **188**, 84–90 (2012). 10.1016/j.juro.2012.02.2572
40. M. Beitzinger, L. Peters, J.Y. Zhu, E. Kremmer, G. Meister, RNA Biol. **4**, 76–84 (2007). 10.4161/rna.4.2.4640
41. Z. Tang, C. Li, B. Kang, G. Gao, C. Li, Z. Zhang, Nucleic Acids Res. **45** (2017). 10.1093/nar/gkx247. W98-W102

# Figures

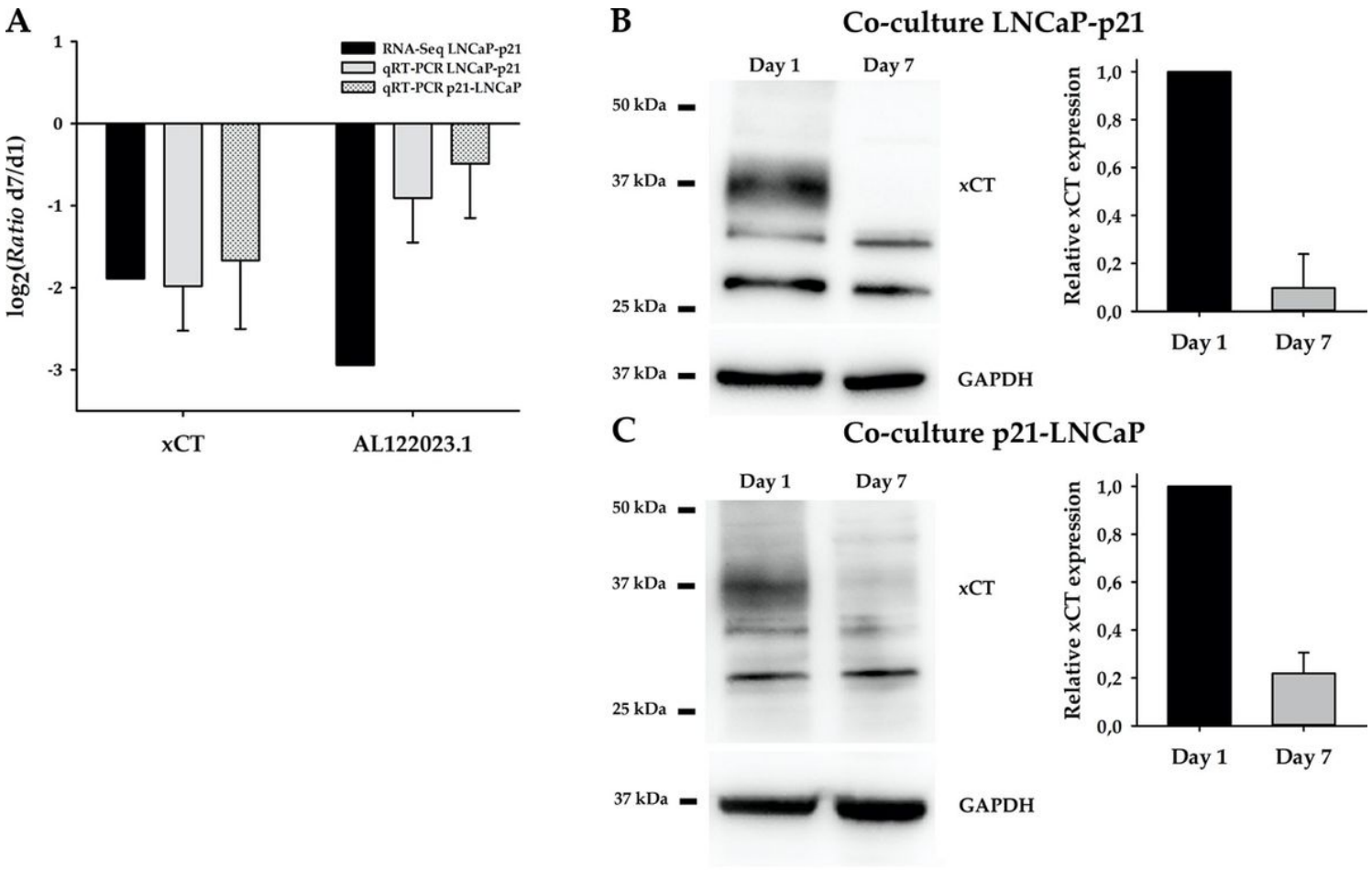


## Figure 1

Analysis of *xCT* and *AL122023.1* expression in LNCaP cells after interaction with stromal p21 cells via soluble factors for seven days. (**A**) RNA sequencing data (black bar, RNA seq LNCaP-p21) are validated in three independent co-culture experiments by qRT-PCR (grey bar, co-culture LNCaP-p21). Additionally, repression of *xCT* and *AL122023.1* is also verified in the reciprocal co-culture (grey dotted bar, co-culture p21-LNCaP). Binary logarithm with standard deviation is displayed (n=3). (**B**) (**C**) xCT (35 kDa) expression change in LNCaP cells is also confirmed on protein level by Western Blotting (n=4) for both co-culture systems. GAPDH (36 kDa) served as loading control. d1, day 1; d7, day 7; 25 kDa, 37 kDa and 50 kDa depict the protein size marker.

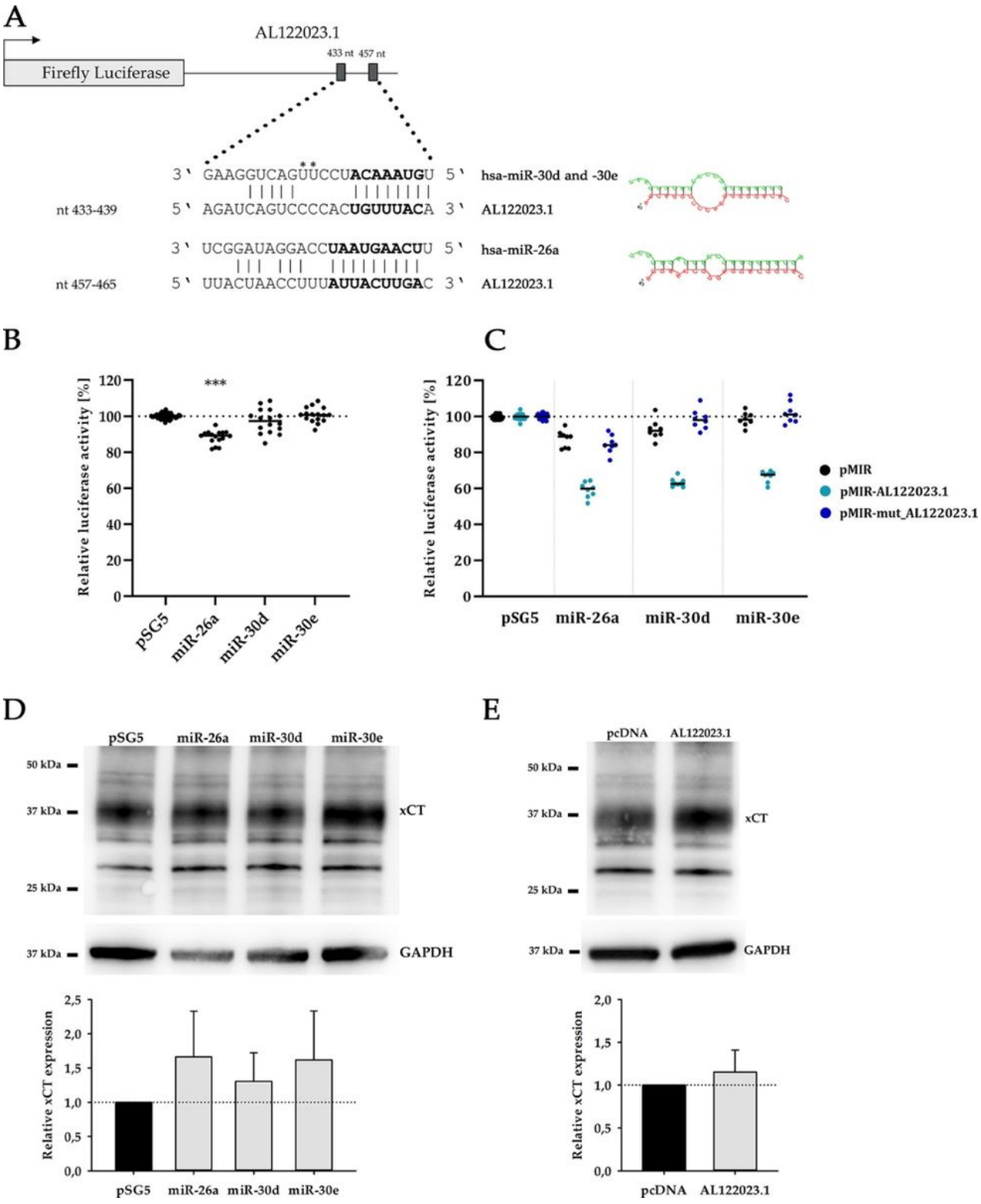


## Figure 2

Mir-26a, miR-30d and miR-30e interact with the lncRNA AL122023.1. (**A**) Schematic illustration of predicted miRNA binding sites within the AL122023.1 sequence. RNAhybrid was used to determine the lowest free energy for hybridization of two RNA molecules (AL122023.1 and miR-30d/e: -20.4 kcal/mol, AL122023.1 and miR-26a 20.7 kcal/mol) and to generate an alternative depiction (right site). *, CC for miR-30d, apart from that identical. The complementary sequences corresponding to the seed sequences

were removed by shortage of the AL122023.1 sequence. (**B**) Luciferase reporter assays were performed to investigate the lncRNA-miRNA-interaction. Control transfections of reporter plasmid (pMIR) with empty effector plasmid (pSG5) were set to 100% (illustrated by dashed line). Only miR-26a shows a significant effect on the reporter plasmid. (**C**) MiR-26a, -30d, and -30e cause a significant reduction in luciferase activity of approximately 30% after interaction with AL122023.1 (pMIR-AL122023.1, light blue) (n=4, measured in duplicates). This effect can be reversed when miRNA binding sites are deleted (pMIR-mut_AL122023.1, dark blue); ***, p<0.001. (**D-E**) Overexpression of miR-26a, -30d, -30e and AL122023.1 in LNCaP cells cause an induction of xCT protein amount. GAPDH (36 kDa) served as loading control. 25 kDa, 37 kDa and 50 kDa depict the protein size marker.

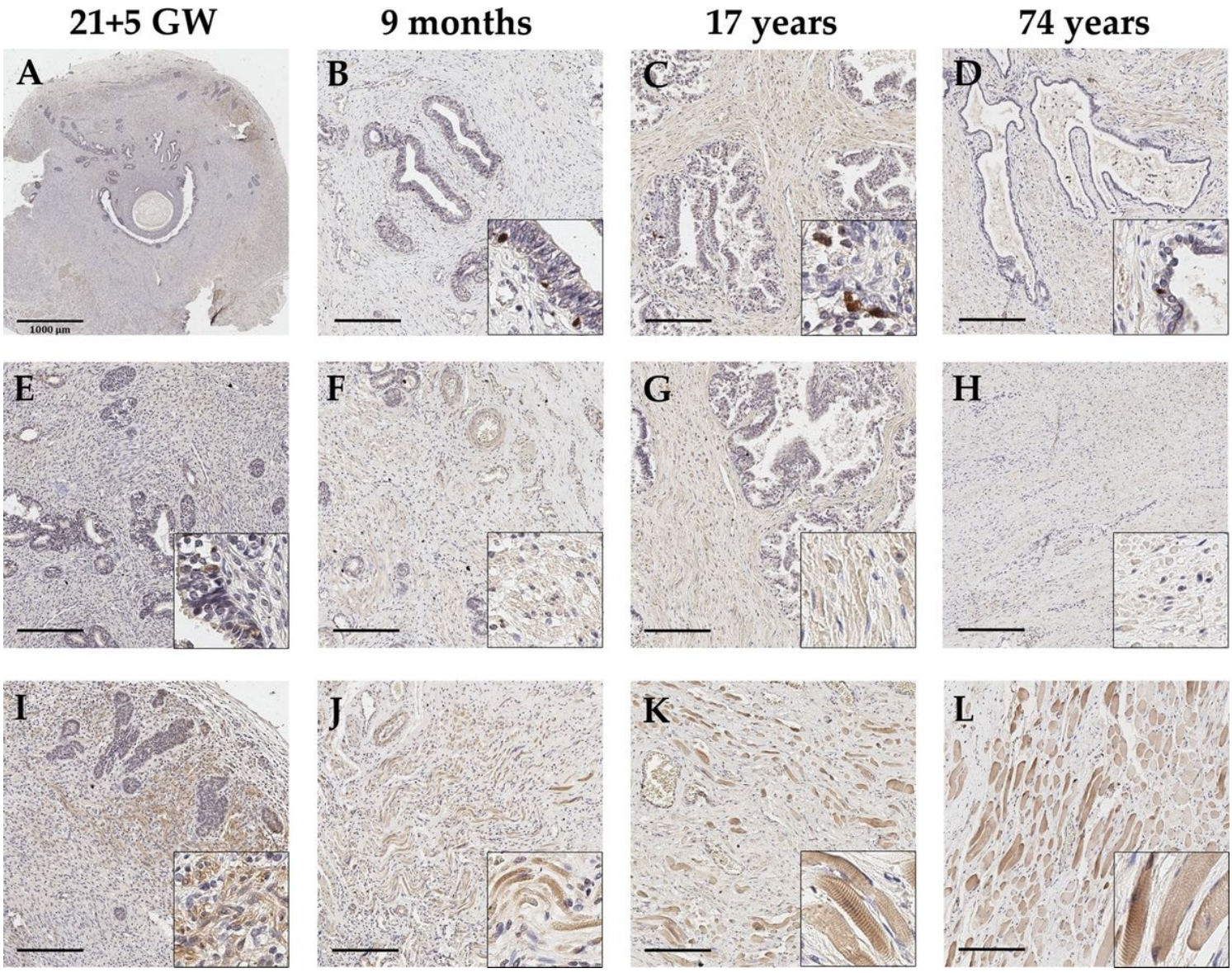


## Figure 3

Representative immunohistochemical staining of healthy prostate tissue differing in age, ranging from fetal over juvenile to adult (column-wise) to detect xCT. (**A-E**) Glandular epithelium is weakly positive for xCT in fetal tissue, whereas postnatal tissue shows distinct strong xCT-positive cells. (**F-I**) In adjacent

stroma a weak to moderate xCT expression is detected. (**J-L**) Present skeletal muscle is steadily strongly xCT-positive. In general, no age-related change can be observed. Scale bar, 200 µm.

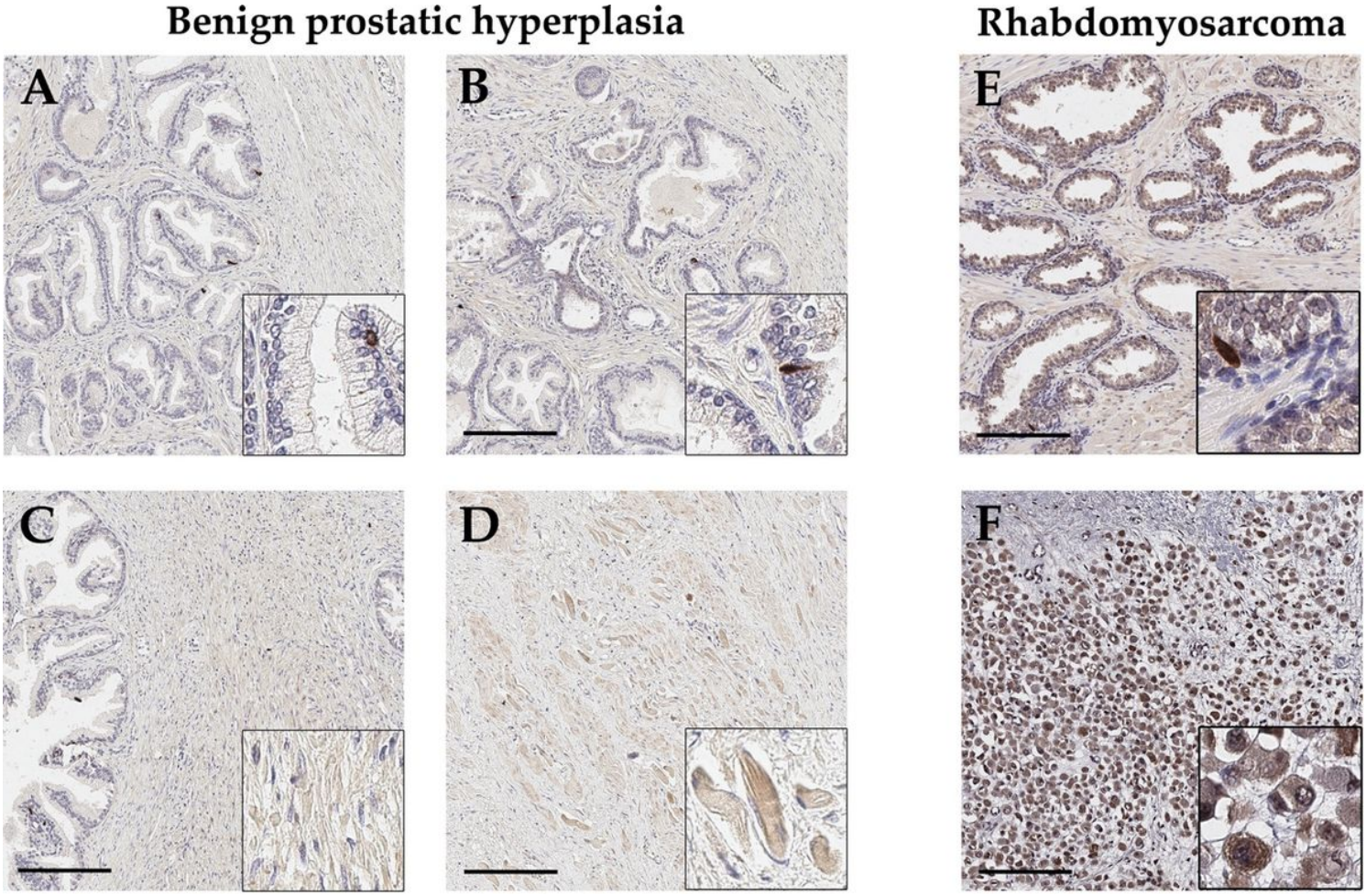


**Figure 4**

Representative immunohistochemical staining of benign prostatic hyperplasia (BPH) and rhabdomyosarcoma with anti-xCT antibodies. (**A-B**) Single cells with an intense xCT expression are detected in glandular epithelium in BPH. (**C-D**) Some stromal cells appear weakly xCT-positive, while skeletal muscle cells display a distinct xCT expression. (**E-F**) In rhabdomyosarcoma, tumor cells strongly express xCT, whereas adjacent normal tissue shows the typical staining of single cells within the glandular epithelium. Scale bar, 200 µm.

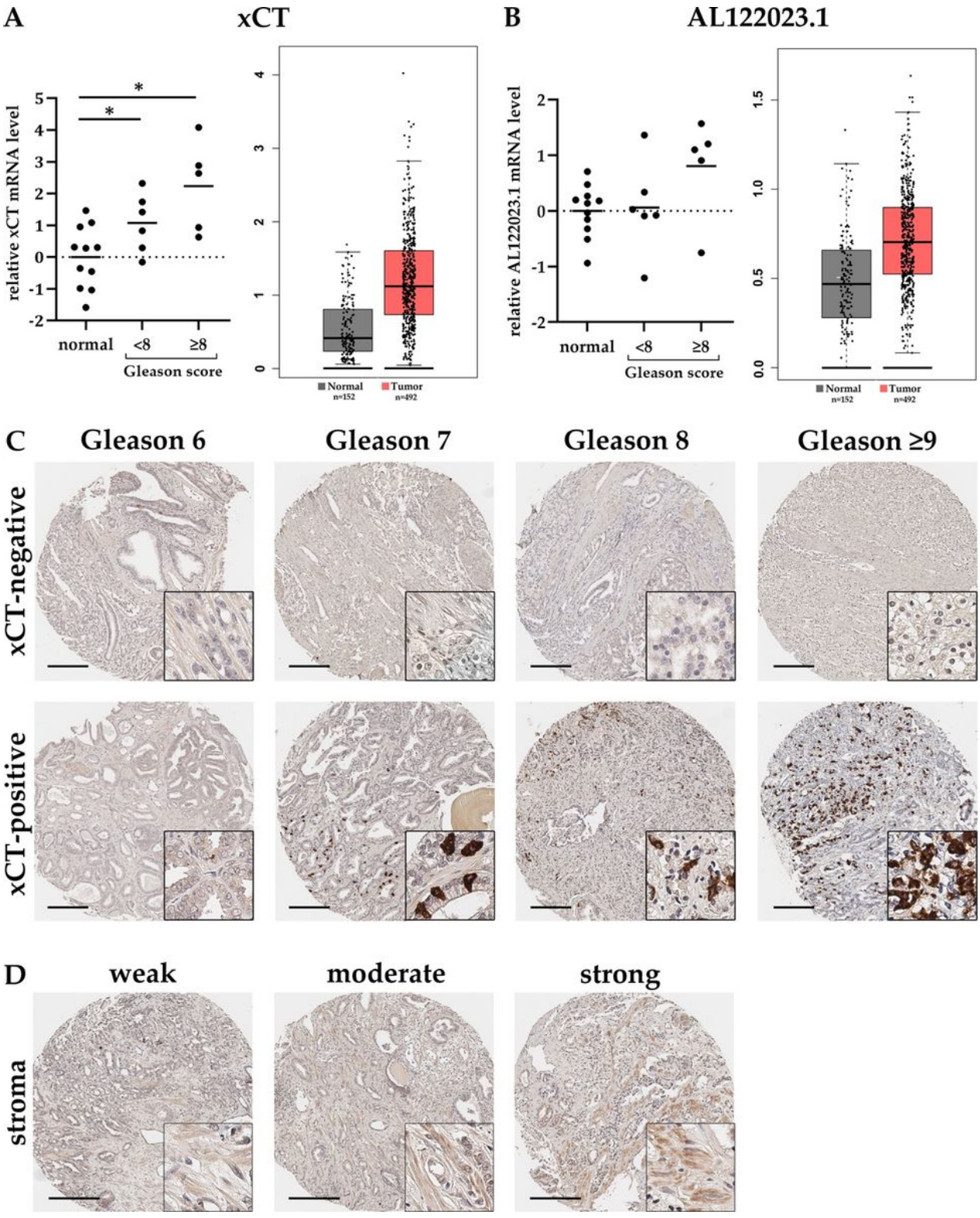


## Figure 5

xCT expression in PCa samples with different Gleason score. (**A**) (**B**) To determine the relative expression change (ratio) of xCT and AL122023.1, cryoconserved PCa samples with Gleason score <8 (n=6) or ≥8 (n=5) compared to adjacent normal tissue (n=11) were used. QRT-PCR results reveal an induction of xCT and AL122023.1 expression with rising Gleason score (unpaired t-test for normally distributed data; ∗ $p<0.05$). Expression in normal tissue is shown as distribution around the mean. HPRT1 and GAPDH both

served as reference genes. Results of the GEPIA Database confirm the induced expression of *xCT* and *AL122023.1* in PCa (visually adjusted graph). (**C**) Tumor microarrays with 196 PCa biopsies with different Gleason scores were assessed after immunohistochemical staining with anti-xCT-antibodies. Two representative samples are shown per Gleason score (6, 7, 8, ≥9) and distinguished between xCT-negative (no detection of cells expressing xCT) and xCT-positive (detection of xCT expression in cells). The number of xCT-positive cells raises starting from Gleason score 7. (**D**) xCT expression was also investigated in associated stroma and samples were classified into absent, weak, moderate, or strong staining as shown in the representative images. Scale bar, 200 μm.

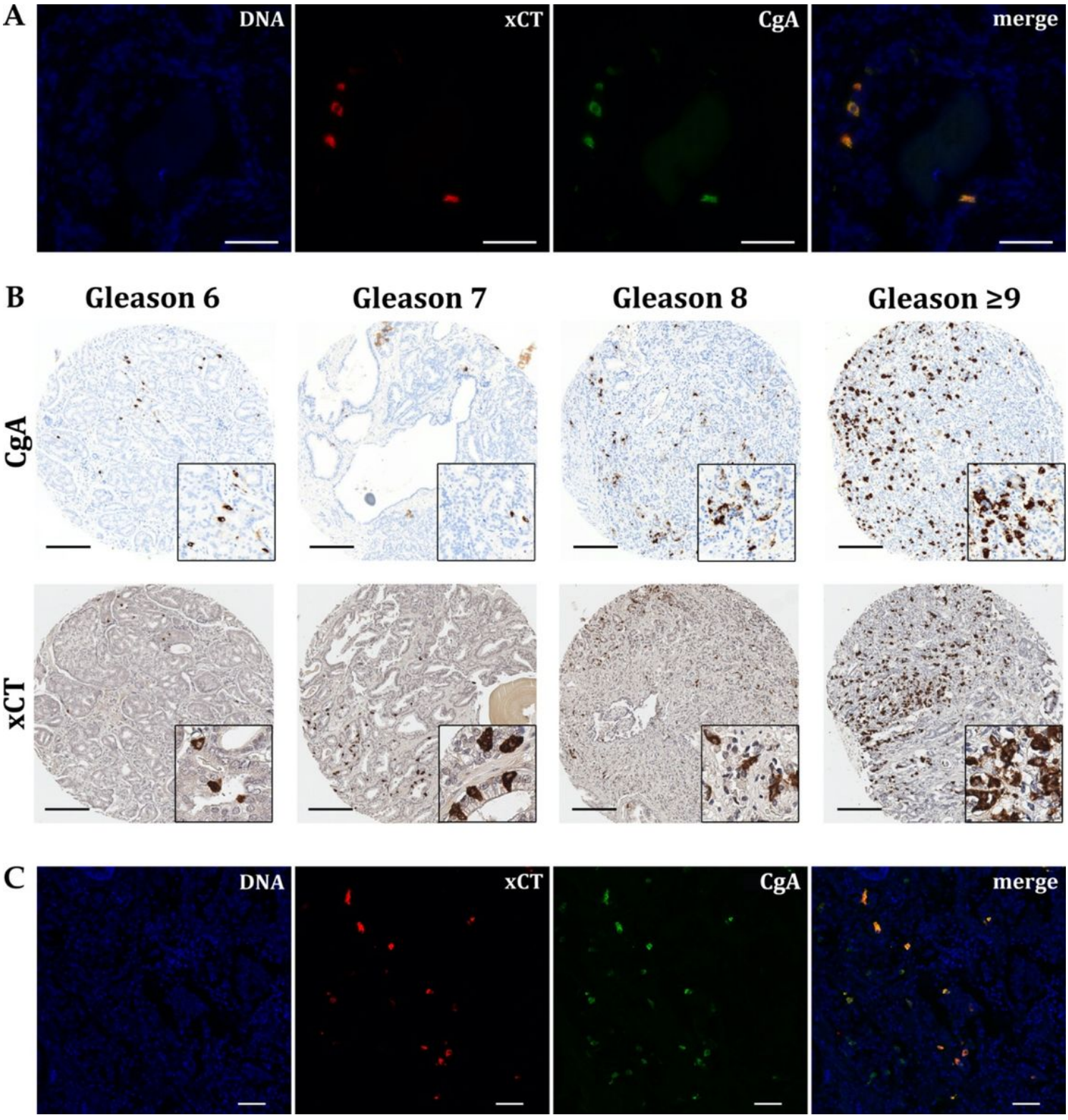


## Figure 6

Examination of cells expressing xCT. (**A**) Double immunofluorescence staining of xCT (red) and CgA (green) in healthy prostate tissue was first performed showing a clear colocalization (merge). The fluorochrome DAPI visualizes DNA in the cell nuclei (blue). Scale bar, 50 µm. (**B**) Detection of xCT and CgA in a selection of PCa biopsies with different Gleason scores (column-wise) from a TMA. Comparison of CgA and xCT shows a similar staining pattern. Morphologic differences result from different

sectioning levels. Scale bar, 200 μm. (**C**) To detect neuroendocrine-like tumor cells in PCa after androgen deprivation therapy, corresponding double immunofluorescence staining were performed (n=5) confirming colocalization of xCT and CgA. Scale bar, 50 μm.

## Supplementary Files

This is a list of supplementary files associated with this preprint. Click to download.

- CellularOncologyPaper2SupplementaryxCTAL122023.1.docx